EXCIMER LASERS

Excimer laser refers to a large class of lasers that use excimer, exciplex, or trimer molecules as the active medium. These molecules form stable compounds only in the excited state, and once de-excited, they dissociate on time scales of the order of 10^{-12} s, which means that the lower laser level is practically always empty. Thus high pump and laser efficiencies are possible. Excimer lasers are pumped by electrical discharges, electron or proton beams, or optical techniques. Today, a large number of lasing excimer compounds are known, spanning a wavelength range from the visible to the vacuum ultraviolet spectral region. Of the many possible active media, rare-gas halide lasers are the most widely applied as powerful, tunable radiation sources in the ultraviolet. Their application fields range from fundamental science to manufacturing and to medicine. This class of excimer lasers is the focus of this article.

The use of excimer molecules as active laser media was proposed as early as 1960. The first excimer lasers, based on rare gas excimers, were demonstrated in the early 1970s by Basov et al. (1), Koehler et al. (2), and Hoff et al. (3). The first rare-gas halide laser was reported by Searles and Hart in 1975 (4), and many other lasing compounds were discovered shortly thereafter. Extensive summaries of the various excimer compounds including their chemistry and spectroscopy are in (5) and (6).

Table 1. Table of Potential Active Media for Excimer Lasers and Their Emission Wavelengths

Type	Active Medium	Wavelength (nm)
Diatomic rare-gas halides	XeCl	253
	XeBr	282
	XeCl	**308**
	XeF	**351**
	KrI	185
	KrBr	206
	KrCl	**222**
	KrF	**248**
	ArBr	161
	ArCl	175
	ArF	**193**
	NeF	308
Triatomic rare-gas halides	Ar_2F	285 ± 25
	Ar_2Cl	245 ± 15
	Kr_2F	400 ± 35
	Kr_2Cl	325 ± 15
	Xe_2F	610 ± 65
	Xe_2Cl	430 ± 40
Rare-gas excimers	Ar_2	126
	Kr_2	146
	F_2	**157**
	Xe_2	172
Metal vapor excimers	HgCl	558
	HgBr	503, 498
	HgIl	444

The examples in bold face have particularly high-gain cross sections and are used in commercial excimer lasers.

Active Media

Excimers and exciplexes form the active media of excimer lasers. They are chemically stable compounds that exist only in the excited state. In a strict sense, excimers are excited dimers made up of two identical subunits, whereas exciplexes are formed by two different compounds. Often, the word excimer is used in the literature for both species. Examples are listed in Table 1. As the name suggests, rare-gas halide excimers consist of a rare gas R and a halide X atom. Typically, there are no stable ground-state RX compounds. The situation is different for the excited state. A reaction of the type

$$R^* + X \rightarrow RX^* \qquad (1)$$

produces a stable molecule in an excited state. This reaction is feasible because R* has a completely different electronic configuration than ground-state R, leading to distinctly different chemical properties. Whereas an R atom has no free valences, R* does and undergoes chemical reactions.

Ground-state, rare-gas atoms Ne, Ar, Kr, and Xe have closed electronic shells with no free (bonding) electrons to form a molecule RX. The electronic configuration of excited-state rare-gas atoms, $^3P_{0,2}$, is very similar to that of an alkali

J. Webster (ed.), *Wiley Encyclopedia of Electrical and Electronics Engineering*. Copyright © 1999 John Wiley & Sons, Inc.

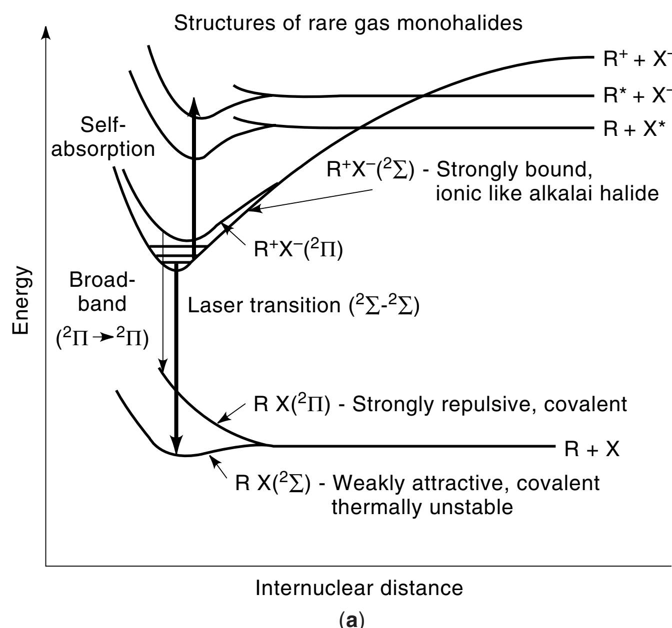

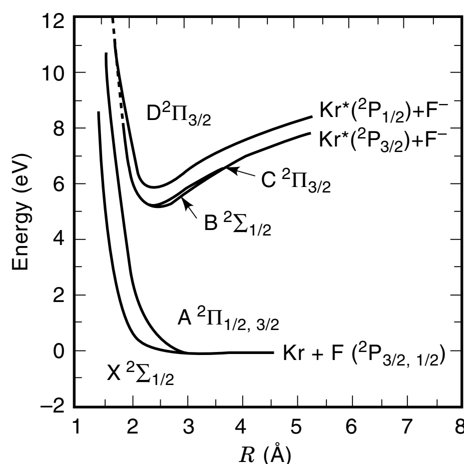

Figure 1. (a) Potential diagram of a rare-gas halide molecule [adapted from (7) by permission]. (b) Energy level scheme of KrF and KrF*, from (8).

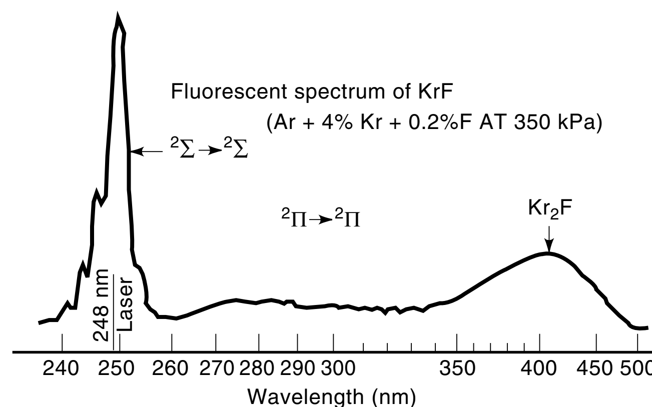

Figure 2. Fluorescence spectrum of KrF* and Kr_2F. Adapted from (7) by permission.

metal, such as Na. In both species, a single electron orbits a positive core, and they subsequently undergo a reaction to form molecules with halide atoms. Depending on which electron is transferred, a molecule in a $^2\Sigma$ or $^2\Pi$ state is formed. The corresponding bond is ionic. The excited rare-gas atoms transfer one charge to the strongly electronegative halide. Thus many properties of the RX* molecules are similar to those of alkali halides. A detailed summary of the binding and potential curves of rare-gas halides is in (7).

Figure 1(a) shows a potential diagram of the electronic structure of the rare-gas halides. Figure 1(b) shows KrF as an example. The ground state comprises a weakly attractive and a repulsive potential which is a consequence of the P-type halogen and the S-type rare gas atom. The binding type is covalent leaving the molecule in either a RX($^2\Sigma$) or RX($^2\Pi$) state. The potential curve belonging to the former is either flat or exhibits a shallow minimum which makes the molecule thermally unstable. The π-bond gives rise to a repulsive potential. The emission spectrum of an excited RX molecule has a distinct maximum and a broad continuum. The former is attributed to the $^2\Sigma \rightarrow {}^2\Sigma$ transition on which lasing is achieved.

The bound molecule decays to the ground state emitting a photon

$$RX^* \rightarrow R + X + h\nu \tag{2}$$

Typical fluorescent lifetimes are on the order of ns to 100 ns. The dissociation of the (unstable) ground-state molecules occurs on a time scale of ps making the lower laser level practically empty, which means that a population inversion between RX* and RX is relatively easy to achieve. The emission cross sections are on the order of 10^{-16} cm^2, comparable with laser dye molecules. The cross section σ_F is estimated from the fluorescent lifetime τ_F and spectral width $\Delta\lambda_F$ (7)

$$\sigma_F \approx 0.04 \frac{\lambda^4}{\Delta\lambda c \tau_F} \tag{3}$$

assuming lifetime broadening and Gaussian transition profiles.

Depending on the pump mechanism and gas composition, several different reactions are possible, leading to a rare-gas halide excimer. As an example, several processes leading to KrF* in a high-voltage, high-pressure discharge containing Kr, F_2, and Ne are listed, following (8). These are the main reactions leading to KrF*:

$$Kr^+ + F^- + Ne \rightarrow KrF^* + Ne$$
$$\text{three-body excimer formation (ionic channel)} \tag{4}$$

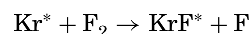

$$Kr^* + F_2 \rightarrow KrF^* + F$$
$$\text{harpooning reaction (neutral channel)} \tag{5}$$

Table 2. Spectroscopic Data of KrF*

Internuclear equilibrium distance	0.23 nm
Vibrational frequency (KrF*)	310 cm^{-1}
Transitional wavelength	248.5 nm
Fluorescent linewidth	2 nm
Spontaneous emission lifetime	7 ns
Stimulated emission cross section	2.4×10^{-16} cm^2

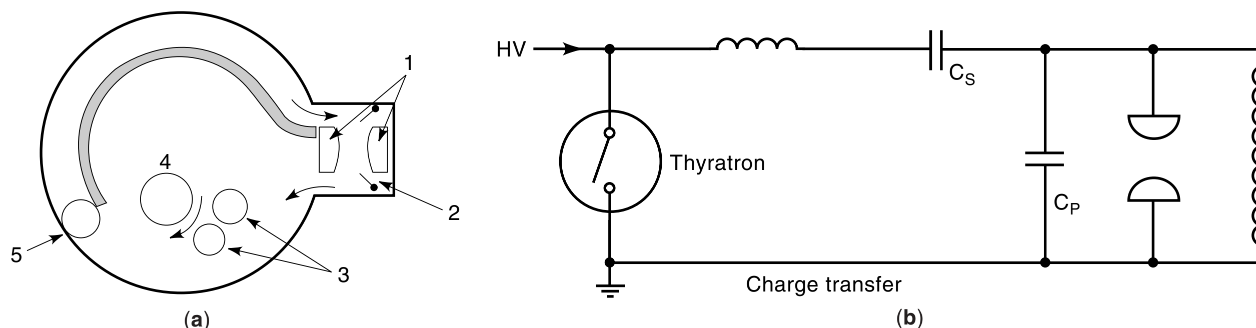

Figure 3. (a) Schematic diagram of an excimer laser discharge chamber. 1-electrodes, 2-preionization pins, 3-heat exchanger, 4-blower, 5-internal cleaning. (b) Electrical discharge circuit (charge transfer circuit). C_s-storage capacity, C_p-peaking capacity.

The ions Kr^+ and F^- and the metastable Kr^* are formed by collisions with electrons:

$$e^- + Kr \rightarrow e^- + Kr^* \quad (6)$$

$$e^- + F_2 \rightarrow F^- + F \quad (7)$$

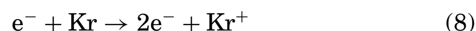

$$e^- + Kr \rightarrow 2e^- + Kr^+ \quad (8)$$

For such an electrical discharge, total pressures between 1 and 3 bar are typical with a relative abundance of the species of Ne:Kr:F ≈ 98.4:1.5:0.1. A manifold of excited KrF states exhibits a potential minimum, a prerequisite for a stable compound. The ground state KrF possesses a dissociative potential which makes KrF an unstable molecule. KrF* decays spontaneously into KrF emitting a photon with a typical lifetime of 5 ns to 10 ns. In contrast the dissociation time of KrF is only a few picoseconds.

Figure 2 shows the fluorescent spectrum of a high-pressure gas mixture. In addition, a three-body collision is likely to occur leading to a triatomic molecule

$$RX^* + 2R \rightarrow R_2X^* + R \quad (9)$$

This reaction gives rise to a broad fluorescent band at longer wavelengths and quenches lasing on the 248 nm line. Table 2 summarizes some spectroscopic data of the transition at 248 nm.

Laser Operation

Pumping. Most commercially available excimer lasers used for industrial and scientific purposes are based on self-sustaining, transverse electrical discharges. To ensure a homogeneous excitation and to prevent filamentation, the active volume is preionized before the main discharge is triggered. Preionization is accomplished, for example, by UV photopreionization where the UV photons are generated by pin-arc or corona discharges. Another possibility is to use X rays to preionize the gas in the discharge volume. The electric discharge circuit is designed for fast discharges (voltage: 20 to 30 kV, current: 30 kA to 50 kA) of durations between 10 and 50 ns. A typical discharge chamber is shown in Fig. 3(a) and a typical discharge circuit in Fig. 3(b). First the storage capacitor C_s is loaded up to the loading voltage, the peaking capacitor C_p is uncharged. Next the thyratron is switched which transfers the charge to the capacitor C_p. When the voltage at C_p reaches the breakdown voltage of the gas mixture, an electrical discharge takes place pumping the active medium. A low inductance of the peaking circuit (a few nanohenries for C_p and 100 nH for the thyratron) guarantees a fast rise time of the discharge. In rare-gas halide lasers, small signal gain coefficients, $g_0 = \sigma_g N$, on the order of 0.1 to 0.2 cm^{-1} are desired, requiring excited molecules at densities of $N \approx 10^{15}$ cm^{-3}. This inversion density determines certain requirements for the pumping process, summarized in Table 3.

Electron beam pumping is applied for very high-power, low-repetition rate laser systems. The (pulsed) electron beam is injected into the laser resonator and is steered and guided with the aid of magnetic fields. Several excitation geometries are possible, comprising longitudinal, transverse, and coaxial pumping (9). The primary excitation process ionizes the buffer gas which distributes the energy in collisions to the rare-gas and halide atoms. Typically an electron beam generated by an accelerator enters the discharge region through a thin window of aluminum or titanium 5 μm to 50 μm thick. A lower limit of the electron energy is caused by losses of about 200 keV in the entrance window. The maximum energy is determined by the maximum efficiency of the energy coupling into the gas. The main advantage of electron beam pumping is the possibility of exciting large gas volumes to produce large laser pulse energies. Output energies of KrF systems of tens of kilojoule are reported (10). Typical pulse durations are between 0.01 and 1 μs. Such lasers are important for laser fusion research.

Small-scale excimer lasers based on waveguide-type active regions are operated at a several kilohertz repetition rate (11). They consist of a radio-frequency source as pump (pump power ~ 10 kW/cm^3), an impedance-matching circuit, and two electrodes between which is placed a small insulating tube (~ 1 mm diameter, 30 mm long) containing the gas. The output pulse energies are typically not larger than a few tens of mi-

Table 3. Pump Parameters for Rare Gas Halide Lasers Required to Reach Small Signal Gain Coefficients of 0.1 to 0.25 cm^{-1}

Discharge current density	~ 10^3 A/cm^2
Discharge electric field strength	5×10^3 V/cm
Pump power density	5 MW/cm^3
Pump energy density	0.2–0.25 J/cm^3
Pump duration	40–50 ns

Table 4. Laser Beam Properties for Different Excimer Laser Resonators

Resonator Type	Beam Divergence (mrad)	Spatial Coherence Length (nm)
Plane mirrors	3–7	0.2–0.5
Unstable cavity	0.1	2–5
Injection seeded	~ diffraction limited	~ beam diameter

crojoules. The walls of the active volume (diameter of the order of millimeter or less) act as waveguides. Output pulse durations up to a few hundred nanoseconds are possible and linewidths as narrow as a few 10 MHz are reported.

Resonator. For many applications excimer lasers with resonators formed by plane mirrors are used. The output beam is multimode, exhibits a strong divergence of several milliradians, and is relatively broadband. Table 4 summarizes the spatial characteristics of excimer laser radiation for various resonator configurations. The divergence is reduced to about 100 μrad with unstable resonators. Because of the small number of cavity round trips (typical outcouplers have transmission coefficients of 80% and higher), the magnification of such unstable resonators must be high (typically 10) (12). Difficulties associated with implementing unstable cavities of high magnification factors are (1) the cavity feedback decreases with increasing magnification ($\propto 1/M^2$); and (2) the coating of the reflecting spot on the defocusing mirror must sustain high intensities. Rare-gas halide lasers have emission spectra with line widths on the order of a few nm because the excimer molecule exists in several vibrational states. Thus the laser output consists of a band comprising the strongest vibrational transitions. The vibrational relaxation (thermalization) times for typical gas pressures are on the order of 100 ps. Because laser pulse durations are on the order of ns, it is possible to extract most of the excitation energy in a narrow laser line. This is important for applications such as high-resolution spectroscopy and UV photolithography. Such laser operation can be achieved by implementing suitable frequency-tuning and selecting elements. For extreme spectral narrowing, prism beam expanders or etalons combined with gratings are applied. Line widths < 0.2 cm^{-1} (< 1 pm) are feasible and have been demonstrated in commercial systems (13,14) which provide mJ energies. By cascading such frequency filters, even narrower laser output is feasible, albeit at the expense of output power. Laser spectra as narrow as 0.02 cm^{-1} at μJ energies were observed (15).

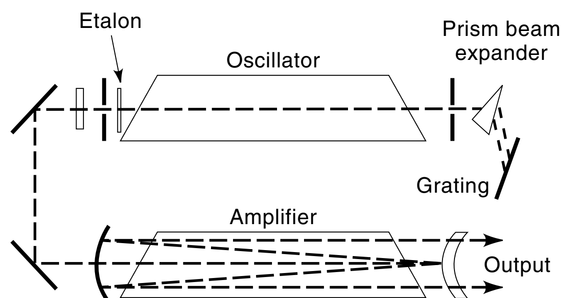

Figure 4. Schematic diagram of an injection-locked unstable resonator. The etalon grating sequence allows frequency narrowing and tuning. The electrical discharges of the two modules need to be synchronized to within 1 ns for optimum performance.

Figure 4 shows an example of a narrowband and injection-locked unstable resonator for an excimer laser.

Excimer Laser Output Characteristics

The main output parameters of typical commercial excimer lasers are listed in Table 5 and illustrated in Figs. 5, 6, and 7. It should also be mentioned that the wavelength of excimer laser radiation can be shifted by nonlinear optical effects. Raman shifts in gases (16) are particularly attractive because of the UV transmissivity and the avoidance of damage effects.

Interaction of UV Laser Radiation with Materials

Fundamentals. The generation, handling, and application of excimer lasers involves interacting powerful UV radiation with matter. At low power the response of the material is completely described by a complex dielectric constant,

$$\epsilon(\omega) = \epsilon_1(\omega) + i\epsilon_2(\omega) \tag{10}$$

or complex refractive index,

$$\tilde{n}^2(\omega) = \epsilon(\omega) = [n(\omega) - i\kappa(\omega)]^2 \tag{11}$$

where n is the (real) refractive index and κ is the imaginary part of the refractive index responsible for absorption. A UV beam incident on a material surface is partly reflected and partly transmitted into the substrate. Under normal incidence the reflection coefficient is given by

$$R(\omega) = \left|\frac{\tilde{n}(\omega) - 1}{\tilde{n}(\omega) + 1}\right|^2 \tag{12}$$

The propagation through the substrate is affected by absorption leading to an exponentially damped intensity $I(z)$:

$$I(\omega, z) = I(\omega, z = 0)e^{-\alpha(\omega)z} \tag{13}$$

where $\alpha = 4\pi\kappa/\lambda$ is the coefficient of small signal absorption. A characteristic penetration depth is defined by $d_p = \alpha^{-1}$.

Table 5. Typical Properties of Excimer Laser Radiation

Output Power	Figs. 5, 6
Pulse energy	Figs. 5, 6
Pulse to pulse stability	0.5–1.5%, Fig. 6(b)
Pulse duration	20 ns, Fig. 6(c)
Beam size	5 mm × 20 up to 50 mm × 50 mm, Fig. 7
Divergence	0.1–0.5 mrad (see Table 4)
Bandwidth	0.5 nm (plane–plane cavity) < 1 pm (line narrowing elements)

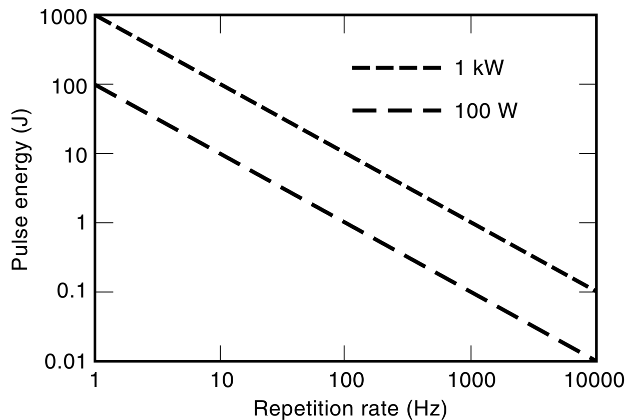

Figure 5. Energy per pulse as a function of repetition rate.

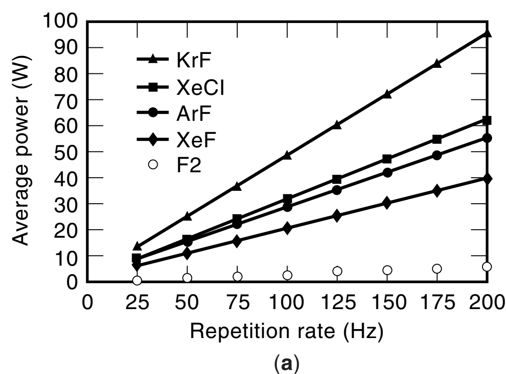

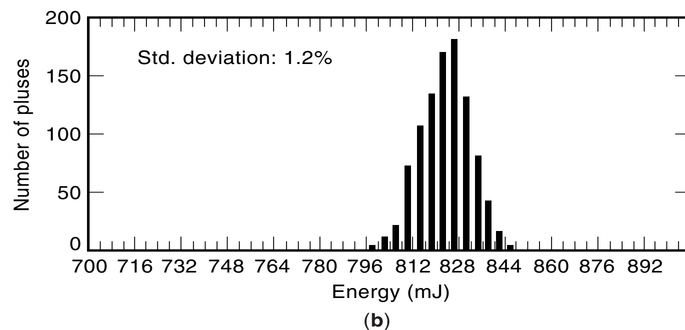

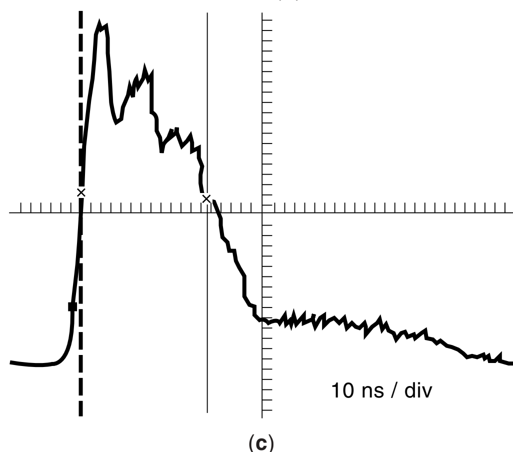

Figure 6. (a) Output power vs repetition rate for different types of excimer lasers. (b) Pulse to pulse stability of a 100 Hz, KrF excimer laser (LPX 210i, Lambda Physik). (c) Temporal profile of a typical Krf excimer laser pulse. The full width at half maximum is 25 ns. From (23).

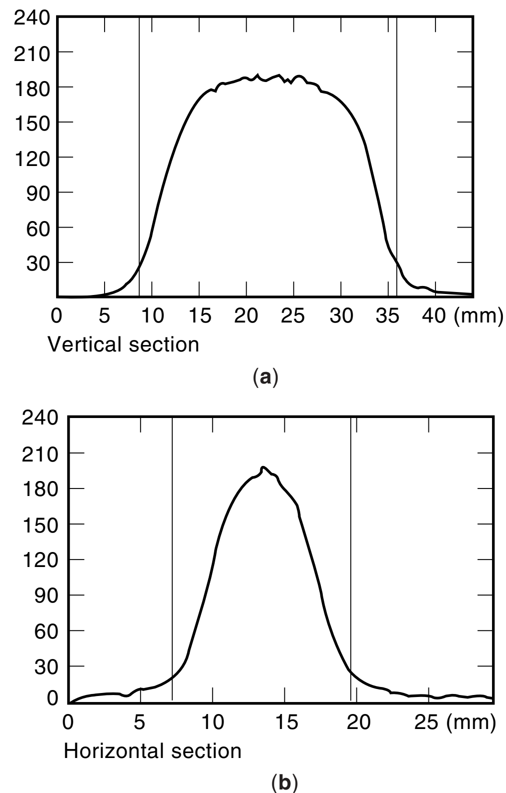

Figure 7. Beam intensity profile in (a) vertical and (b) horizontal direction of a KrF excimer laser (ComPex 205, Lambda Physik). From (23).

Nonlinear absorption occurs at high input intensities. A corresponding process of nth order is described by an absorption coefficient

$$\alpha^{(n)} = \text{const.} \times I^{n-1} \tag{14}$$

Absorption of UV light is generally accompanied by excitation of the electronic system through interband transitions in insulators (wide-gap materials) and semiconductors and interband and intraband transitions in most metals.

Optical Components. Optical components with high UV light transmission are needed as outcouplers, beam splitters and focusing optics, for example. Ordinary glass materials are not suitable because of their large absorption in the UV. Table 6 shows some materials used for high-transmission optical components in the UV and their transmission limit determined by the bandgap. At high (pulse) intensities the absorption becomes nonlinear (see Eq. (14)) and, in addition, longer lasting absorption centers like color centers and defects occur.

For reflection optics, dielectric multilayer mirrors are mostly used with reflectivities exceeding 99%. Wide-gap oxide and fluoride compounds with high transmission in the UV serve as coating materials. High-reflection layers are a sequence of alternating high and low refractive index quarter-wave coatings. Typical combinations are HfO_2/SiO_2 and LaF_3/MgF_2. A common problem with high-power laser radiation is laser damage. Progress in the layer fabrication enabled coatings with damage thresholds above 10 mJ/cm^2 when exposed to 20 ns KrF laser pulses. Metal mirrors (e.g., alumi-

Table 6. Examples of Materials Used for Optical Components at Excimer Laser Wavelengths

Material	Band Gap (nm)	n(308 nm)	n(248 nm)	n(193 nm)
SiO_2 (SQ1)	159	1.4856	1.5086	1.562
Crystal quartz	138	1.486	1.508	1.562
MgF_2	105	1.405	1.41/1.405	1.466/1.451
CaF_2	124	1.46	1.457	1.501
BaF_2	136			
LiF_2	107	1.382	1.412	1.445
Al_2O_3	150			

num) are low cost alternatives, but reflectivities do not exceed 90% at excimer laser wavelengths.

Interaction of UV Light with Strongly Absorbing Materials

Absorption Processes. Most industrial UV laser applications remove materials after absorption of laser radiation. At excimer laser wavelengths the absorption is caused by resonances of the electronic system. Many materials exhibit a large absorption coefficient. As a result the excimer radiation is absorbed in a thin surface layer. At sufficiently high excitation energies the deposited energy density is so high that a material surface layer is ablated. The physical mechanisms involved are manifold and depend on material, excitation wavelength, and pulse energy and duration. One can roughly divide these processes into photothermal and photochemical mechanisms.

In metals, UV photons are absorbed by free electrons occupying states near the Fermi level. With absorption coefficients α on the order of 2×10^6 cm^{-1}, the absorption length (skin depth) d_p is only a few nanometers. This means that the energy of a UV laser pulse minus the reflection loss is deposited in a small surface layer. This quantity $(1 - R)$ is shown for some materials and typical excimer wavelengths in Table 7. It is interesting to note that these numbers are about one magnitude larger than achieved with CO_2 lasers at 10.6 μm in the infrared spectral region. Depending on the metal (work function) and photon energy (laser wavelength), a certain fraction of the excited electrons are ejected out of the material, cooling the metal. The remaining excitative events populate higher states in the metal, and are followed by fast electron–electron collisions and finally electron–phonon and electron-impurity scattering, leading to material heating. These processes proceed on a time scale of a few picoseconds and less. The resulting temperature distribution evolves according to the following heat conduction equation:

$$\nabla^2 T(\vec{r}, t) - \frac{1}{\gamma}\frac{\partial T(\vec{r}, t)}{\partial t} = -\frac{S(\vec{r}, t)}{K} \quad (15)$$

where $S(\vec{r}, t) = (1 - R)I_0(t)\alpha e^{-\alpha z}$ is the source term due to the incident laser intensity I_0, K is the thermal conductivity, and γ is the thermal diffusivity. With laser pulses, the heat generation rate can exceed the dissipation due to diffusion by many orders of magnitude resulting in heating the sample up to the melting temperature. Continuous heat supply can exceed the latent heat to melt a surface layer, and further heating and vaporization occurs. This type of thermal material removal is the essential mechanism of processing metals.

In semiconductor and insulators absorption takes place via interband transitions. Intraband transitions in the upper band associated with electron–phonon scattering lead to material heating. In addition impurity centers, excitons, and defect states provide additional absorption centers for photon energies below the bandgap energy. Table 8 shows the fraction $(1 - R)$ and the absorption coefficient for some semiconductors.

A different mechanism dominates the interaction of UV laser light and organic materials such as polymers, for example. The absorption of UV photons leads directly to bond breaking and to photodissociation of one or more components of the material. The resulting gas and radicals are ejected from the material surface. Unlike the thermal processes previously described, photodissociation does not exhibit a threshold. The incident photon energy only has to exceed the bond dissociation energy E_b. Table 9 gives some examples. At high enough input intensities, multiphoton (n-photon) absorption occurs which leads to photodissociation if $n\hbar\omega \geq E_b$.

Material Removal (Ablation). In media where photothermal effects play the major role, laser-controlled material removal proceeds via melting and evaporating surface layers. To obtain the surface temperature, one has to solve Eq. (15) where the source term is determined by the absorbed laser intensity, $S = (1 - R)I_{in}(\vec{r}, t)e^{-\alpha z}$. Because the lateral dimensions are

Table 7. Fraction of the Incident Fluence (Incident Minus Reflected) Absorbed in a Thin Surface Layer

Material	308 nm	248 nm	193 nm
Ag	0.89	0.74	0.74
Au	0.63	0.66	0.76
Co	0.51	0.60	0.64
Fe	0.59	0.67	0.73
Ni	0.58	0.54	0.64
Ti	0.47	0.60	0.64

Data from (18).

Table 8. Fraction of Incident Fluence Absorbed in a Thin Surface Layer $(1 - R)$ and Absorption Coefficient α of Some Semiconductors at Typical Excimer Laser Wavelengths

	$1 - R$			α	(10^6 cm^{-1})
Material	308 nm	248 nm	193 nm	308 nm	248 nm
Ge	0.44	0.35		1.50	1.62
Si	0.41	0.33		1.54	1.81
GaP	0.55	0.42		0.88	1.84
GaAs	0.58	0.33		0.78	2.07
PbS	0.53	0.62	0.82	0.92	0.82
InSb	0.39	0.46		1.50	1.24

Data from (18).

Table 9. Dissociation Energy and Corresponding Photon Wavelengths of Some Bonds

Bond	E_b (eV)	λ (nm)
H_2	4.48	277
O_2	5.12	243
CO	11.09	112
C—C	3.62	343
C=C	6.4	194
C≡C	8.44	147
C—H	4.30	289

Data from (18).

much larger than the absorption lengths α^{-1}, $\nabla^2 \approx (d^2/dz^2)$ in Eq. (15). For a uniform incident intensity $I_{in}(x, y, z = 0) = I_0$ and $(t\gamma)^{-1/2} \gg \alpha^{-1}$, Eq. (15) is then solved analytically and yields the temperature profile. For the temperature increase at the material surface we find, see for example, (17), that

$$T(z=0,t) = \frac{2}{K}(1-R)I_0\left(\frac{\gamma t}{\pi}\right)^{1/2} \qquad (16)$$

For a numerical example let us assume that $t = 20$ ns (typical excimer pulse duration at 248 nm), a gold target with $(1 - R) \approx 0.66$, $\gamma \approx 1.3$ cm²/s, K ≈ 3 W/cm/K, and $\alpha \approx 10^6$ cm^{-1}. With these numbers we obtain a surface temperature increase of about 2 K per mJ/cm². A 100 mJ excimer laser pulse focused on a spot of 1 cm² would thus increase the surface temperature by about 200 K.

After the melting temperature is reached, continuous energy supply leads to melting, additional heating, and evaporation. From thermodynamical considerations [see, e.g. (18)], maximum ablation rates in metals are about 0.01 m/s at sufficiently high excitative energy densities. For typical excimer laser pulses (20 ns) this amounts to about one atomic layer per pulse. In reality energy deposition is more complex and observed ablation rates are considerably larger. Depending on the target material, they reach values of several μm per pulse at incident fluences of several J/cm². Several processes occur simultaneously during the incident laser pulse and affect the absorption process and material removal. For example, a mechanical reaction of the expanding laser-induced vapor with the molten material can lead to rapid

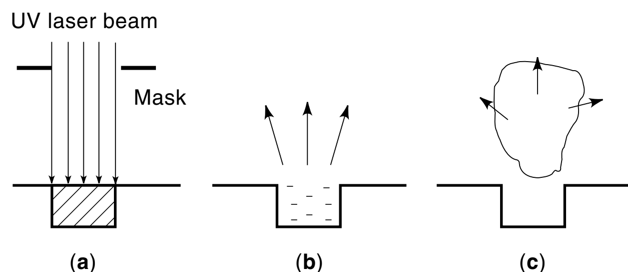

Figure 8. Schematic diagram of the ablation process. (a) Energy deposition (excitation/heating) in an absorbing surface layer. (b) Bond breaking (direct deposition/thermal vibrational excitation) and explosive expansion. The ejected particles leave the surface nearly perpendicularly with velocities exceeding 2000 m/s. (c) A hot cloud of ablated material with neutral and ionized particles is produced and expands.

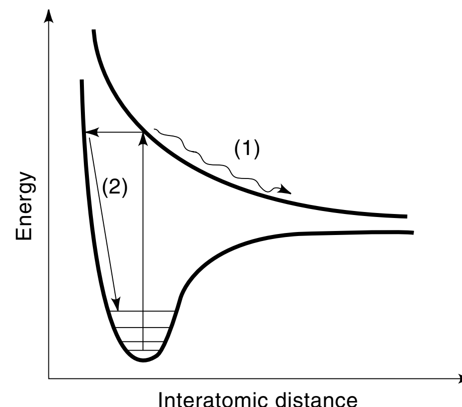

Figure 9. Simplified picture of the two channels [photochemical (1) and photothermal (2)] that initiate ablation processes after excitation of the electronic system of a polymer.

removal of the liquid. In this case, the ablation depth corresponds roughly to the material depth in which the melting temperature is reached. The material removal initially increases with increasing laser fluence, reaches a maximum, and then decreases at higher fluence. This effect is attributed to laser-supported detonation. The laser heats the vapor which in turn expands rapidly, preventing further efficient energy deposition into the target.

In organic materials, material removal with ultraviolet laser pulses proceeds witout extensive heating (photoablation). The UV photon energy is large enough to break bonds. The fragments are initially under high pressure and are ejected from the surface thereby carrying away the deposited energy as kinetic energy. This "cold" material removal takes place within one absorption length and provides a controllable tool for material removal. Because the surrounding material is hardly affected, the ablated area distinguishes itself by sharp boundaries.

Figure 8 shows a schematic diagram of the ablation process involving an interplay of photothermal and photochemical processes. As mentioned above, ablation is a very complex process, and many questions still remain to be explored. Fig-

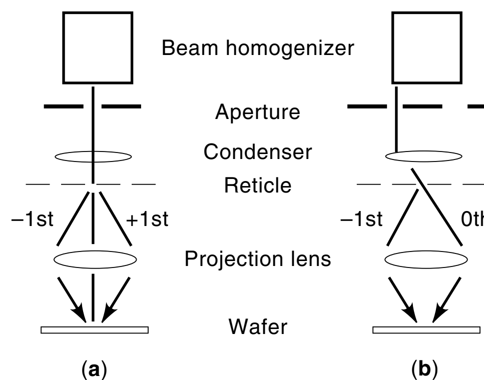

Figure 10. Stepper illumination arrangement for deep UV lithography. (a) conventional illumination; (b) illumination with an annular aperture. For a given projection lens, the application of an annular aperture increases the effective numerical aperture of the system compared with conventional illumination.

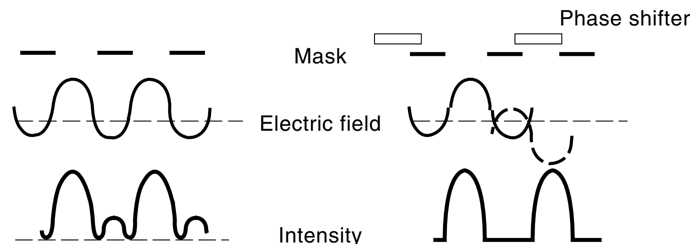

Figure 11. Schematic diagram of the function of a conventional and a phase-shifting mask. Destructive interference between the fields from two adjacent apertures avoids undesired intensity maxima in the shadow region.

ure 9 is an example of how photochemical (dissociation) and photothermal processes occur in one and the same type of species (a polymer in this case) after UV photon absorption. Channel 1 is the direct photochemical decomposition starting from the excited electronic state without thermal effects. Channel 2 proceeds via relaxation through the vibronic ladder (after internal conversion) of the ground state heating the sample to the melting point. Pure photochemical ablation, due to the absence of heating, results in steeper edges and allows for better resolution.

It should also be mentioned that incubation effects exist in organic materials with relatively small absorption coefficients, that is, the ablation does not start with the first illumination pulse but only after a certain number of incubation pulses are absorbed.

Application Examples

Excimer lasers are broadly applied in various fields ranging from fundamental research to manufacturing.

Industrial and Medical Applications. Industrial applications of excimer lasers involve ablation, UV microlithography, micromachining, annealing, metal deposition, and laser cleaning to name a few of the most important areas.

Excimer Laser Assisted Chemical Etching. The idea behind laser assisted chemical etching is to efficiently remove material layers in the presence of a precursor gas that chemically reacts with the material. Depending on the gas and material, several processes are feasible. They involve the formation of radicals in the gas after UV photon absorption and subsequent chemical reaction with the material and desorption. The latter can also be enhanced by the UV laser. Compared with ablation the necessary fluences are considerably smaller. Submicron spatial resolution is possible by controlling the intensity profile of the incident laser beam.

Deep UV Lithography with Excimer Lasers. In photolithography for microelectronics, a mask is demagnified and imaged onto a photoresist, typically a polymer, which is then chemically processed to produce the desired structures. The excimer laser is the radiation source for a high-resolution optical projection aligner, the so-called wafer stepper or scanner. Excimer lasers are an ideal tool for photolithographic purposes for several reasons. The short wavelengths provide potential resolutions of better than 100 nm. The high pulse fluences allow for short exposure times and even simultaneous illumination of large areas (wafers) without scanning. For the next few years excimer lasers will remain the main tool in the microelectronic industry for the fabrication of integrated circuits, notably microprocessors and memory chips. Because of the immense importance of this technology we will go into somewhat more detail here.

Table 10. Structural Sizes Achieved by Photolithography with Excimer Lasers

Wavelength	Regular Structures (memory chips)	Random Structures (microprocessors)
248 nm	$< 0.2\ \mu$m	0.25 μm
193 nm	0.13–0.18 μm	0.18 μm

Table 11. Data for Commercial Excimer Lasers Used for Deep UV Lithography

	KrF	ArF
Laser efficiency (broadband)	2.5%	1.3%
Narrowing efficiency	30%	$< 10\%$
Repetition rate	1 kHz	600 Hz
Output power	10 W	5 W
Tuning range	248.4 $\pm$ 0.15 nm	193.35 $\pm$ 0.15 nm
Bandwidth	0.6–0.8 pm	0.7 pm
Wavelength stability	$\pm$0.1 pm	$\pm$0.1 pm
Energy fluctuations	$< 3\%$	$< 5\%$

Resolution and Depth of Focus. The performance of a photolithographic system is largely determined by depth of focus and lateral resolution. The resolution or minimum structure dimension that can be realized is

$$\Delta d = \frac{\delta_d \lambda}{\text{NA}} \tag{17}$$

where λ is the illumination wavelength and NA is the numerical aperture of the projection lens or system, and δ_d is a empirical factor depending on the optical system and the resist material. The depth of focus is given by

$$\Delta z = \frac{\partial_z \lambda}{(\text{NA})^2} \tag{18}$$

where δ_z is an empirical factor characteristic for a certain projection optics and resist. Typical imaging systems have numerical apertures of 0.5 to 0.6. The field sizes of lenses have

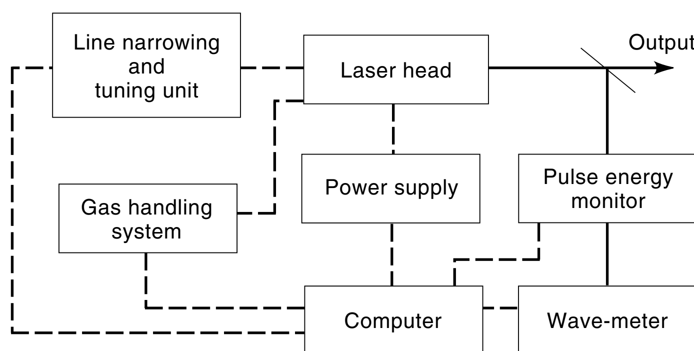

Figure 12. Schematic diagram of a commercial excimer laser used for industrial photolithography.

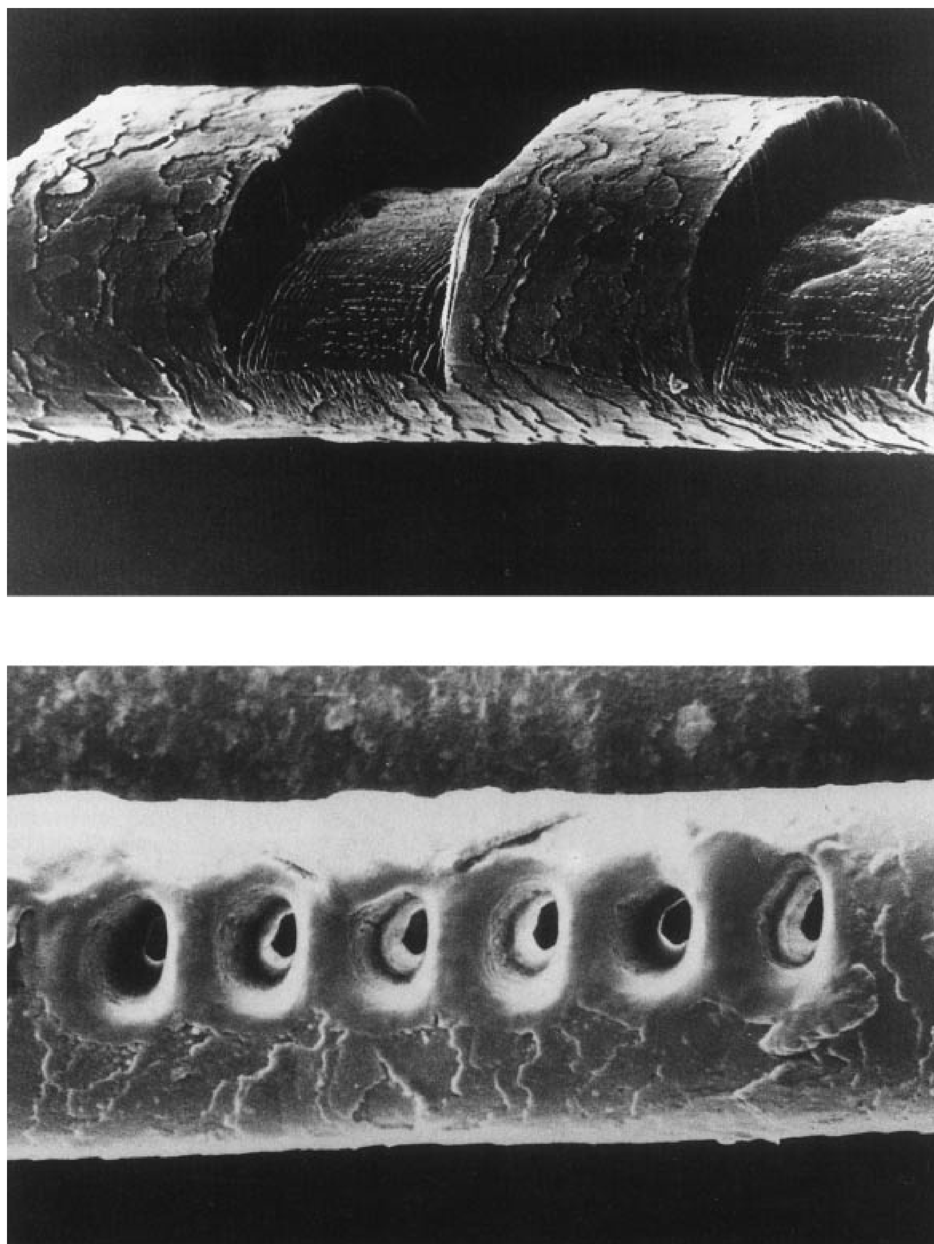

Figure 13. Scanning electron micrographs of structures cut into a human hair using excimer laser micromachining. (Courtesy Lambda Physik GmbH.)

been increased from 10 to > 20 mm^2. The δ-factors (a typical value for 248 nm and 193 nm lithography is 0.5) can be lowered through: (a) the application of a high contrast photoresist, (b) the use of annular illumination (see Fig. 10), and (c) the employment of phase-shifted masks (see Fig. 11). To homogenize the beam, different spatial components are mixed. This, for example, can be achieved by a system of fly's eye lenses or a fused silica rod with highly reflecting walls. With deep UV lithography employing KrF and ArF excimer lasers structures with dimensions of less than 250 nm are possible. With ArF lithography (193 nm) the production of 4 and even 16 Gbit memory chips seems to be feasible. Table 10 summarizes the achievable resolutions.

Projection Lenses. There are two different types of projection systems—all refractive optics, and catadioptic reflective-refractive systems. All-refractive imaging systems consist only of lenses. The most critical type of aberration is chromatic aberration. To reduce this effect very narrow-band excimer lasers are necessary. For demagnification factors of 5 to 10 all refractive optics (made from fused silica) require laser bandwidths of 0.8 pm at 248 nm and 0.3 pm at 193 nm. At 193 nm a reduction of chromatic aberration can be achieved by using a combination of fused silica and CaF_2 lenses which can accomodate bandwidths of 0.7 pm. The conditions are further relaxed for catadioptic systems which call for 100 pm at 248 nm and 20 pm at 193 nm. Catadioptic systems are made of reflecting components only and thus exhibit smaller chromatic aberrations. Table 11 summarizes the current status of narrowband excimer lasers which are suitable for all-refractive projection systems which is the most widely used concept today. The spectral narrowing is achieved through prisms and gratings as detailed in the section on resonators. A schematic diagram of a state-of-the-art excimer laser used for lithography is shown in Fig. 12.

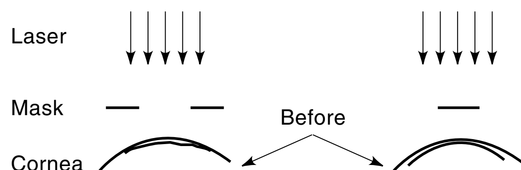

Figure 14. Schematic diagram of photorefractive keratectomy. Depending on the mask structure, the central or outer parts of the cornea are illuminated with excimer laser radiation. The subsequent ablation leads to a reshaping of the cornea, that is, to a change in its radius of curvature. This allows correcting near and farsightedness.

Laser Hardening and Annealing. Hardening steel surfaces requires heating above the martensitic transition point and subsequent quenching by cooling. A short laser pulse is ideal to locally excite (heat) a thin surface layer. Then the cooling is accomplished by rapid heat diffusion into the bulk material.

Annealing of semiconductors to heal structural damage from ion implantation is of great concern in fabricating electronic components. Again the material is heated by a laser pulse up to a temperature where the atoms rearrange. Depending on the duration of the illuminating pulse, this process can occur before actual melting takes place.

Laser Vapor Deposition. Laser deposition is very attractive for generating high-quality, thin films. The idea is to focus the excimer laser on a target composed of the material to be deposited on a substrate. The excimer laser pulse causes ablation leading to a plume of gas that propagates to the substrate where it is adsorbed as a thin film.

Micromachining. Material removal with excimer lasers is widely applied in micromachining. There are two major techniques used. One is to place a mask in contact with the object to be processed. Relatively large areas can be processed simultaneously unlike with Nd:YAG or CO_2 laser where scanning is usually applied. Pulse fluence and number of pulses determine the amount of material removal. An alternative schema involves a high-quality projector that demagnifies a mask onto the material surface by an excimer laser beam. Precise drilling and cutting with submicron resolution is possible. Two examples that demonstrate this are shown in Fig. 13.

Excimer Laser Application in Medicine. Excimer lasers are increasingly applied in various fields of medicine. One of the most advanced developments is in opthalmology in corneal surgery. The controllable and localized material removal provided by excimer laser radiation permits a predefined reshaping of the cornea to correct vision defects such as farsightedness and nearsightedness (see, for example (19).

A schematic diagram is shown in Fig. 14. With ArF excimer lasers, ablation depths per pulse range from 0.01 μm at 50 mJ/cm^2 to 1 μm for flows above 700 mJ/cm^2 (19). The absorption of UV light takes place mostly in the peptide bonds of collagen molecules, the most abundant organic molecule in the corneal tissue. This bond occurs in concentrations of about 10^{21} cm^{-3} and has a molar extinction coefficient of 5.5×10^3 cm^{-1}M^{-1}. Bond breaking is followed by a microexplosion on the corneal surface leading to ejection of debris. Heating of the cornea is minor. Cell membranes and other protein-based organic materials shield the cell nuclei from UV radiation and prevent potential damage (mutation) to the DNA.

Applications in Science

Pump Source for Other Lasers. Excimer lasers are used uniquely in fundamental and applied science as a source of powerful pulses in the UV. Because many molecules have broad absorption bands in the UV, excimer lasers are used to pump other lasers, notably dye lasers. A schematic diagram is shown in Fig. 15(a). A cell filled with an organic dye solution is pumped transversely by an excimer laser. The resonator is formed by an outcoupling mirror and a grating. The latter serves for frequency tuning and bandwidth narrowing. To increase the resolution, the beam is expanded before impinging on the grating. If higher output powers are required, such an oscillator is supplemented by a second dye cell acting as an amplifier. Many different oscillator configurations have been developed depending on the desired output parameters. A few different dyes cover the whole spectral range from the near-UV to the visible to the near-infrared [see Fig. 15(b)]. Such tunable dye laser systems have been broadly applied in high-resolution spectroscopy (20). In recent years though they have been replaced by solid-state laser-pumped optical parametric oscillators (OPO). Typical pulse durations are a few ns with line widths of a few hundred megahertz. Systems based on short-cavity and distributed-feedback dye lasers have been developed to generate pulses as short as a few hundred femtoseconds (21). Frequency-doubled femtosecond pulses at 308 nm and 248 nm have been amplified in XeCl and KrF excimer

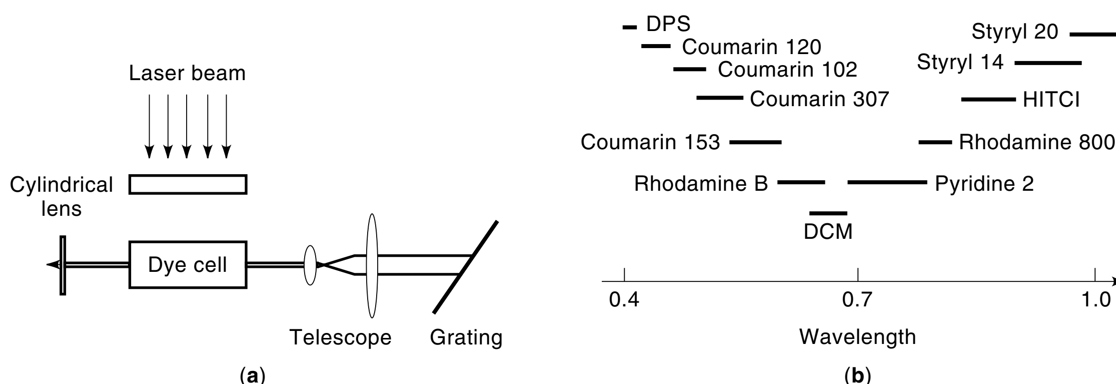

Figure 15. (a) Schematic diagram of an excimer laser pumped dye laser. (b) A few dyes pumped by a XeCl excimer laser at 308 nm cover the spectral range from the near IR to the near UV. Data from (24).

gain modules leading directly to femtosecond pulses with millijoule energies in the UV with pulse durations as short as 50 fs (see, for example, (22)). Such pulses are used in time-resolved spectroscopy and to generate short pulses in the vacuum UV and X-ray spectral range, to name just a few applications.

Spectroscopy with Excimer Lasers. Because of large photon energies, excimer lasers are well suited to excite and ionize electronic transitions in many organic and inorganic molecules. If excitation is followed by fluorescence, sensitive detection schemes can be applied that allow detection of small concentrations of species. Such methods are important for environmental remote sensing, for example. If excitation leads to ionization, mass spectroscopy is applied to identify the photofragments with high sensitivity. Application fields are surface analysis (desorption) and cluster physics, to name just a few areas.

BIBLIOGRAPHY

1. N. G. Basov et al., Laser operating in the vacuum region of the spectrum by excitation of liquid xenon with an electron beam, *JETP Lett.,* **12**: 329, 1970.
2. H. A. Koehler et al., Stimulated VUV emission in high-pressure xenon excited by high-current relativistic electron beams, *Appl. Phys. Lett.,* **21**: 198, 1972.
3. P. W. Hoff, J. C. Swingle, and C. K. Rhodes, Observation of stimulated emission from high-pressure krypton and argon/xenon mixtures, *Appl. Phys. Lett.,* **23**: 245, 1973.
4. S. K. Searls and G. A. Hart, Stimulated emission at 281.8 nm from XeBr, *Appl. Phys. Lett.,* **27**: 243, 1975.
5. Ch. K. Rhodes (ed.), *Excimer Lasers.* Berlin, Heidelberg, New York, Tokyo: Springer Verlag, 1984.
6. M. H. R. Hutchinson, Excimer lasers, in L. F. Mollenauer and J. C. White, (eds.), *Excimer Lasers.* Berlin: Springer Verlag, 1987.
7. C. A. Brau, Rare gas halogen excimers, in C. K. Rhodes, (ed.), *Excimer Lasers,* Berlin: Springer, 1984.
8. U. Rebhan and D. Basting, Excimer lasers: Current status and future developments, *Ber. Bunsenges. Phys. Chem.,* **97**: 1504, 1993.
9. M. Obara and F. Kannari, Rare gas-halide lasers, in R. A. Meyers (ed.), *Encyclopedia of Lasers and Optical Technology,* San Diego, CA: Academic Press, 1991, pp. 568–586.
10. A. M. Hunter II, R. O. Hunter, and T. R. Johnson, Scaling of KrF lasers for inertial confinement fusion, *IEEE J. Quant. Electron.,* **QE-22**: 386, 1986.
11. C. P. Christensen et al., High-repetition-rate XeCl waveguide laser without gas flow, *Opt. Lett.,* **12**: 169, 1987.
12. T. J. McKee, B. P. Stoicheff, and S. C. Wallace, Diffraction-limited KrF and XeF lasers with a negative branch unstable resonator, *Appl. Phys. Lett.,* **30**: 278, 1977.
13. H. Endert, R. Paetzel, and D. Basting, New KrF and ArF excimer lasers for DUV lithography, *Microelectron. Eng.,* **27**: 221, 1995.
14. J. Kleinschmidt et al., Extremely narrow-bandwidth, high-repetition rate laser for high NA step and scan tools, *SPIE 1996 Int. Symp. Microlithography,* Santa Clara, 1996.
15. J. Goldhar, M. W. Taylor, and J. R. Murray, An efficient double-pass Raman amplifier with pump intensity averaging in a light guide, *IEEE J. Quantum Electron.,* **QE-20**: 772, 1984.
16. J. C. White, Stimulated Raman scattering, in L. F. Mollenauer and J. C. White, (ed.), *Tunable Lasers.* Berlin: Springer-Verlag, 1987.
17. H. S. Carslaw and J. C. Jaeger, *Conduction of Heat in Solids.* Oxford: Oxford University Press, 1986.
18. W. W. Duley, *UV Lasers: Effects and Applications in Materials Science,* Cambridge: Cambridge University Press, 1996.
19. G. H. Pettit, M. N. Ediger, and R. B. Weiblinger, Excimer laser ablation of the cornea, *Opt. Eng.,* **34**: 661–667, 1994.
20. W. Demtröder, *Laser Spectroscopy,* Heidelberg: Springer, 1996.
21. S. Szatmari and F. P. Schaefer, Subpicosecond widely tunable distributed feedback dye laser, *Appl. Phys.,* **B46**: 305–311, 1988.
22. J.-C. Diels and W. Rudolph, *Ultrashort Laser Pulse Phenomena: Fundamentals, Techniques, and Applications on a Femtosecond Time Scale.* San Diego: Academic Press, 1996.
23. Lambda Physik Excimer Lasers: The UV solution for scientific, medical and industrial applications, 1997, Lambda Physik GmbH, Technical Information.
24. U. Brackmann, *Lambdachrome Laser Dyes,* Lambda Physik GmbH, Goettingen, 1994.

J. W. Nicholson
W. Rudolph
University of New Mexico
J. Kleinschmidt
Lambda Physik GmbH